STRUCTURE AND INFRASTRUCTURE ENGINEERING
https://doi.org/10.1080/15732479.2020.1759658



# Performance assessment of prestressed concrete bridge girders using fiber optic sensors and artificial neural networks

Omid Khandel[a], Mohamed Soliman[a], Royce W. Floyd[b] and Cameron D. Murray[c]

[a]School of Civil and Environmental Engineering, Oklahoma State University, Stillwater, OK, USA; [b]School of Civil Engineering and Environmental Science, University of Oklahoma, Norman, OK, USA; [c]Department of Civil Engineering, University of Arkansas, Fayetteville, AR, USA

**ABSTRACT**

Structural health monitoring (SHM) activities are essential for achieving a realistic characterisation of bridge structural performance levels throughout the service life. These activities can help detect structural damage before the potential occurrence of component- or system-level structural failures. In addition to their application at discrete times, SHM systems can also be installed to provide long-term accurate and reliable data continuously throughout the entire service life of a bridge. Owing to their superior accuracy and long-term durability compared to traditional strain gages, fiber optic sensors are ideal in extracting accurate real-time strain and temperature data of bridge components. This paper presents a statistical damage detection and localisation approach to evaluate the performance of prestressed concrete bridge girders using fiber Bragg grating sensors. The presented approach employs Artificial Neural Networks to establish a relationship between the strain profiles recorded at different sensor locations across the investigated girder. The approach is capable of detecting and localising the presence of damage at the sensor location without requiring detailed loading information; accordingly, it can be suitable for long-term monitoring activities under normal traffic loads. Experimental laboratory data obtained from the structural testing of a large-scale prestressed concrete bridge girder is used to illustrate the approach.

**ARTICLE HISTORY**
Received 19 September 2019
Revised 28 November 2019
Accepted 30 December 2019

**KEYWORDS**
Damage assessment; concrete; prestressed; statistical analysis; sensors; bridges; girders; Artificial Neural Networks

## Introduction

Due to various deterioration processes (e.g. corrosion and fatigue), more than 10% of bridges in the United States are categorised as structurally deficient (FHWA, 2016). Among those, approximately 53% are multi-beam/girder bridges. A large number of newly constructed bridges in the United States use prestressed concrete. In order to facilitate informed repair and replacement decisions when these structures approach the end of their service life, they could be instrumented, during construction, with sensors that can provide accurate and reliable data throughout the entire service life. In this context, fiber Bragg grating (FBG) sensors can provide outstanding long-term stability and highly reliable strain and temperature measurements with minimal processing effort (Lin, Chang, Chern, & Wang, 2004). These sensors, when embedded into the prestressed concrete (PSC) components during construction, can provide accurate real-time strain and temperature measurements at any time during the service life. The measurements obtained from these sensors can be used to assess the initial strain levels from the prestress forces and to develop a baseline strain profile under normal traffic loads that can help in evaluating the long-term condition of the bridge component. Statistical damage detection techniques can be used to achieve this goal by identifying the deviation of a future state of the system from the baseline state (Gres et al., 2017).

The introduction of the fiber FBG sensors by Morey, Meltz, and Glenn (1990) opened the door for applying fiber optic sensors in strain-based performance monitoring activities. Dunphy, Meltz, Lamm, and Morey (1990) demonstrated the feasibility of using FBG sensors in monitoring the response of layered graphite/epoxy composite components. Prohaska et al. (1993) employed FBG sensors to measure strains in a large-scale reinforced concrete beam under pure bending. Research on the application of fiber optic sensors in health monitoring of structures covers other applications including quantifying the short- and long-term changes in the response of concrete structures (e.g. Idriss, Kodindouma, Kersey, & Davis, 1998; Inaudi & Vurpillot, 1999; Lin et al., 2004), studying structural vibration characteristics (Chung & Kang, 2008; Kang, Kim, & Han, 2007), and detecting concrete cracking. FBG sensors have also been used to quantify prestress losses (Abdel-Jaber & Glisic, 2019; Butler, Gibbons, He, Middleton, & Elshafie, 2016) and long-term effects due to creep and shrinkage (Webb et al., 2017).

Fiber optic sensors have also been used for damage detection in PSC components. Zhang, Gao, Shi, Cui, and Zhu (2006) employed fiber optic sensors to identify the damage in externally prestressed concrete T-beams by

CONTACT Mohamed Soliman mohamed.soliman@okstate.edu School of Civil and Environmental Engineering, Oklahoma State University, Stillwater, OK 74078-1010, USA.

comparing their recorded response to analytically derived limit states. Uva, Porco, Fiore, and Porco (2014) proposed a method to identify damage in prestressed concrete viaducts based on expected theoretical strains and actual ones recorded with FBG sensors. Abdel-Jaber and Glisic (2015) used long-gauge FBG sensors to detect pre-release cracks and monitor prestressing force transfer in PSC girders. Their approach focused on damage due to crack opening during the pre-release phase. Waeytens et al. (2016) applied model updating techniques for damage detection in a post-tensioned concrete beam under static loading using distributed fiber optic sensors. Their method, which requires detailed loading information, updates physical parameters (e.g. modulus of elasticity) of different subdomains in a finite element model to match the experimental results. Anastasopoulos, De Smedt, Vandewalle, De Roeck, and Reynders (2018) used FBG sensors to develop strain mode shapes and identify structural damage based on the change in top-to-bottom strain ratio in a prestressed concrete roof girder. However, their approach is more suitable for isolated individual structural components.

Statistical damage detection can be performed using supervised or unsupervised methods. The former method requires damage-sensitive features (DSFs) from both damaged and undamaged states of the structure, while unsupervised methods detect the damage using information from a baseline undamaged structural state (Santos, Crémona, Orcesi, & Silveira, 2013). Due to the fact that obtaining DSFs from the damaged state of the structures is challenging, common statistical damage detection practices often rely on unsupervised methods (Jin & Jung, 2018). Several methodologies are available for damage detection and localisation in bridges using unsupervised statistical damage detection (e.g. Mattson & Pandit, 2006; Reiff, Sanayei, & Vogel, 2016; Weinstein, Sanayei, & Brenner, 2018). However, these methods are often based on small-scale laboratory tests on idealised structures or may require comprehensive finite element analysis and detailed loading information for proper damage detection. In addition, less focus has been placed on the application of unsupervised statistical damage identification in PSC bridge components using fiber optic sensing systems. In particular, an approach capable of assessing damage in PSC bridge components under random loading is required.

This paper presents a framework for damage detection and localisation in newly constructed prestressed concrete bridge girders using fiber optic sensing and Artificial Neural Networks (ANNs). The presented approach uses an inferred relationship between the strain profiles at different sensors distributed across the girder to detect damage under variable amplitude loading. The presented damage detection and localisation approach does not require applied loads as input parameter or detailed finite element analysis of the investigated component. In addition, it has higher accuracy compared to other monitoring techniques relying on foil-type strain gages. The approach is illustrated using experimental data obtained from flexural testing of a large-scale prestressed concrete girder instrumented with FBG sensors. The strain readings obtained during an initial random loading stage are used to train ANNs and define acceptable prediction error bounds to judge whether or not the girder is damaged. The trained ANNs are then used to predict strain profiles at target sensors for other randomly generated variable amplitude and monotonic load tests. Finally, the error between the predicted strains and experimental data is compared to acceptable error bounds to identify and localise the damage in the girder during subsequent load tests.

## Damage detection and localisation procedure

### *Artificial Neural Networks*

ANNs are algorithms designed to recognise numerical patterns. Several types of neural networks, such as feedforward, radial basis function, convolutional, recurrent, and modular neural networks, have been introduced to assist in solving complex computational problems in various research areas (Mehta, 2019). Owing to their superior prediction accuracy and computational efficiency, feed forward ANNs, which consist of one or more hidden layers, have been among the most widely adopted network types (Montana & Davis, 1989). ANNs consist of input, output, and hidden layers. An input layer is responsible for introducing the input parameters ($\mathbf{X}$) to the ANN. The Output layer is the last layer of neurons that streamlines the results matrix ($\mathbf{Y}$), while g hidden layers ($h^{(1)}$ to $h^{(g)}$), each consisting of several neurons (e.g. ${n_1}^{(1)}$ to ${n_{a1}}^{(1)}$ for hidden layer one and, ${n_1}^{(g)}$ to ${n_{ag}}^{(g)}$ for hidden layer $g$), are responsible for converting the input units to nonlinear functions of linear combinations of weights (e.g. ${w_{1,a2}}^{(2)}$ for weights between neuron 1 of first hidden layer and neuron $a2$ of the second hidden layer) and bias values (e.g. ${b_{a1,a2}}^{(2)}$ for bias between neuron $a1$ of first hidden layer and neuron $a2$ of the second hidden layer) assigned to a given input parameter.

A transfer function ($f$) will then determine the state of each hidden layer during the training as (Montana & Davis, 1989):

$$h^{(p)} = f\left[\mathbf{W}^{(p)}\mathbf{X} + \mathbf{B}^{(p)}\right] \text{ and } p = 1 \text{ to } g \tag{1}$$

where $\mathbf{W}^{(p)}$ and $\mathbf{B}^{(p)}$ are the matrices of the weights and bias values associated with the transformation through neurons in hidden layer $p$, respectively. Comparing the ANN prediction to the target output, the assigned weights and bias values are optimised such that the prediction error is minimised.

Feedforward ANNs are known as networks with no closed-loops, meaning that data moves only in one direction from the input nodes, through the hidden nodes, and to the output nodes. Figure 1 shows a generalised layout of a multilayer feedforward ANN. These networks often benefit from a backpropagation algorithm that calculates the gradient of the error with respect to the assigned weights and bias values for a given input. Levenberg-Marquardt (Levenberg, 1944; Marquardt, 1963) nonlinear least squares optimisation algorithm is adopted in this paper for ANN

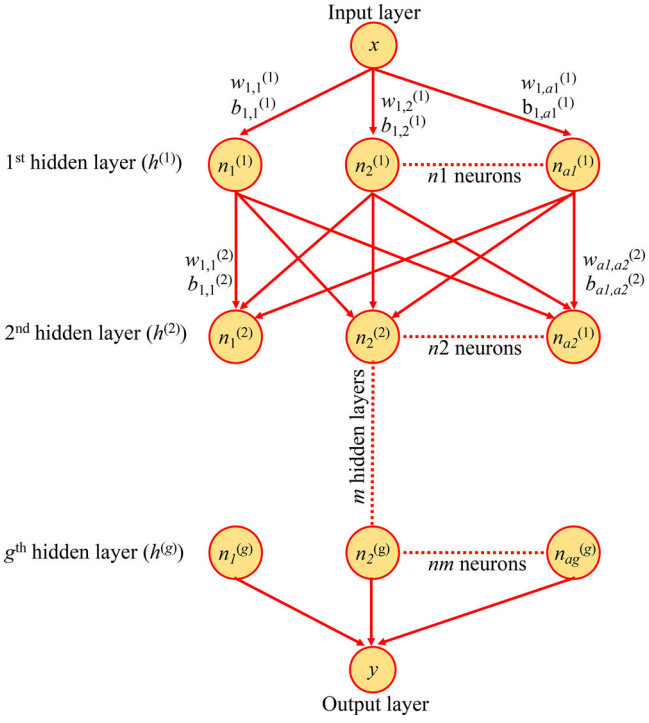


Figure 1. Generalised layout of multilayer feedforward ANNs.

training. This method is well known for its high efficiency and fast convergence (Hagan & Menhaj, 1994).

### Damage detection using ANNs

The approach developed in this paper employs ANNs to establish a relationship between the strains recorded under normal traffic loads by the FBG sensors embedded along the girder. After establishing this relationship, future strain responses recorded under normal traffic loads can be used to identify whether or not the beam is damaged. The proposed framework is designed to identify the damage based only on the strain records without relying on information about the magnitude of applied loads. Several ANNs are trained and tested in order to account for modelling uncertainties associated with their prediction.

The adopted criteria for defining each ANN are discussed in more detail later in this paper. Each individual ANN is trained using a randomly selected sample of the training dataset. The relationship between the strain records of sensors can be different due to the dissimilar nonlinear fit that each ANN establishes. The strain records of all except one sensor (i.e. the target sensor) along the beam are used as the input of the ANNs to predict the strain at the target sensor. After training the ANNs, other available strain records collected during future monitoring, referred to as the set-aside dataset, are fed to the trained ANNs to predict the expected strains at the target sensor. Finally, damage is assessed by comparing the ANN predicted strain response to the actual response obtained by the FBG sensors. Figure 2 shows the layout of the proposed damage detection framework.

To assess the damage occurrence, prediction error is used to compare the simulated strains against those recorded under next load applications. The prediction error associated with individual ANNs at different time instants is:

$$E(i,j) = \varepsilon_{ANN}(i,j) - \varepsilon_{\exp}(i) \tag{2}$$

where $E(i,j)$ is the error associated with $j^{th}$ ANN at the $i^{th}$ time instant, $\varepsilon_{exp}$ $(i)$ is FBG strain record at target sensor associated with the $i^{th}$ time instant, while $\varepsilon_{ANN}$ $(i,j)$ is the strain predicted by the $j^{th}$ ANN at the same time. $n$ and $m$ represent the total number of ANNs and strain data points, respectively. The mean prediction error $ME$ is:

$$ME = \frac{\sum_{j=1}^{n}\sum_{i=1}^{m}E(i,j)}{m \times n} \tag{3}$$

In addition, the mean lower and upper bounds of the strain prediction error associated with the trained ANNs at 95% confidence intervals are:

$$E_{LB} = ME + \frac{\sum_{j=1}^{n}E_{2.5}(j)}{n} \tag{4}$$

$$E_{UB} = ME + \frac{\sum_{j=1}^{n}E_{97.5}(j)}{n} \tag{5}$$

where $E_{LB}$ and $E_{UB}$ are the lower and upper bounds of prediction error associated the testing dataset, respectively, $E_{2.5}(j)$ and $E_{97.5}(j)$ are the 2.5$^{th}$ and 97.5$^{th}$ percentiles of the prediction error associated with $j^{th}$ trained neural network and testing dataset. A damage is detected if the mean prediction error under a specific loading condition falls outside the defined bounds, otherwise the beam is considered undamaged. Note that the defined bounds should be established for the undamaged state of the structure. This is due to the fact that these bounds will be used as a baseline to compare the future behaviour of the girder and identify the potential presence of structural damage. In this paper, these bounds are defined based on Weinstein et al. (2018).

Note that the proposed approach is designed to detect damage in newly constructed bridge girders. In such applications, the ANNs will be only trained once, during the undamaged (i.e. pre-cracking) state of the girders and after installing the girders in place. Although there is no need for continuous training of the ANNs, there is a need for regular analysis of strain records to assess the presence of damage in the monitored component. This process should to be conducted for each monitored girder. Due to the uncertainties associated with material properties, variation in sensor locations, and unforeseen construction conditions, girders with identical design specifications can have different relationship between the strain responses of embedded sensors. In addition, the approach can be also applied to existing bridge girders that are: (a) in an undamaged state and (b) instrumented using any sensor type capable of providing continuous strain readings under variable amplitude loading at several locations along their length.

### Damage localisation using ANNs

To localise damage in PSC girders, the beam is divided into several regions. For each region, a configuration of ANN

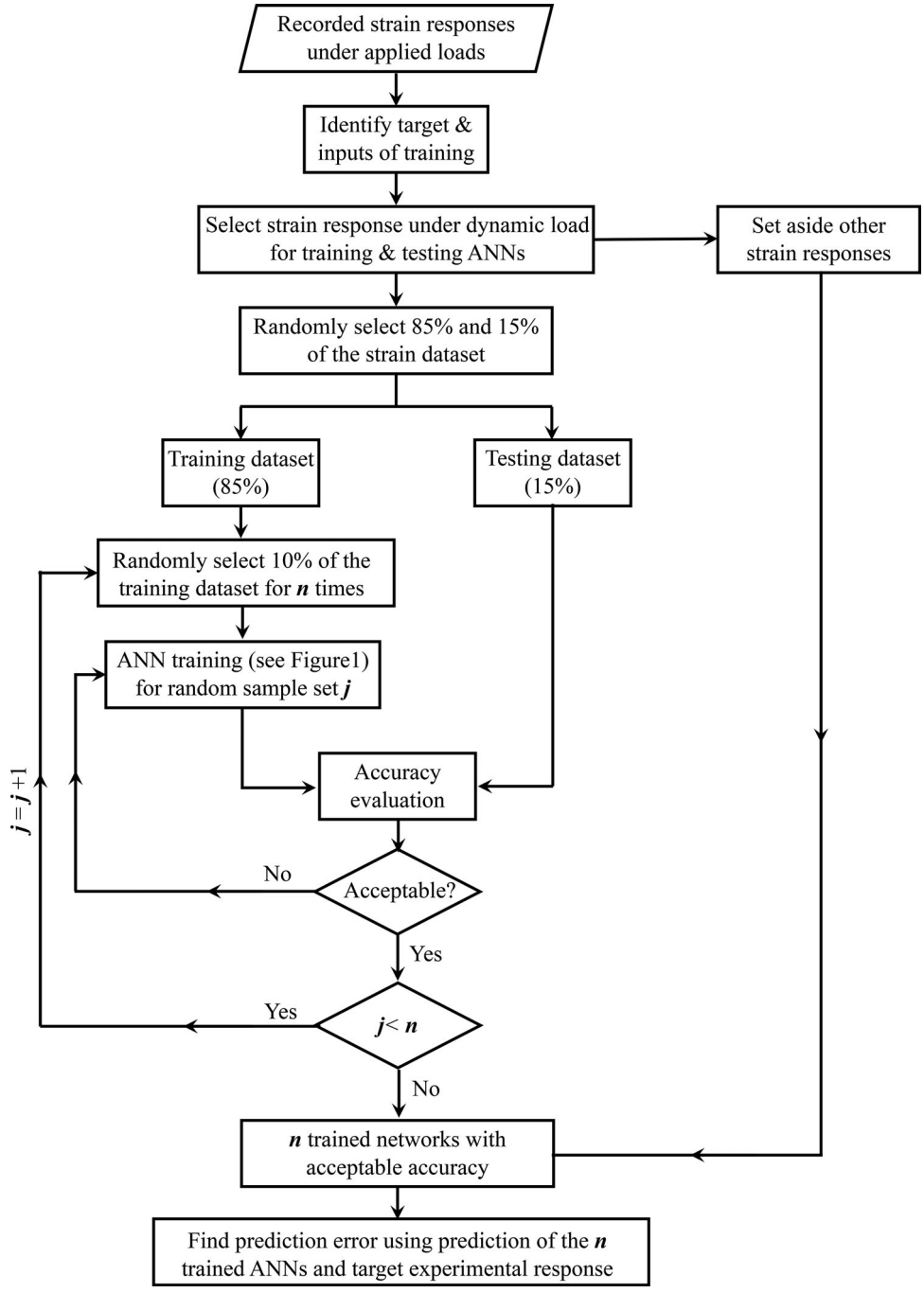


**Figure 2.** Layout of the proposed damage detection framework.

with unique selection of input and target sensors responsible for predicting damage is developed. The flowchart of the proposed damage localisation approach is presented in Figure 3. Strain readings in the undamaged state are used to train the ANNs for different configurations corresponding to regions 1 to ***l***. Eighty-five percent and 15% of the strain records are randomly selected and defined as training and testing datasets. A number of ANNs ($n$) are next trained for each configuration corresponding to defined regions. Each of the $n$ ANNs is then trained using a randomly selected 10% of the training dataset. This process is repeated for the considered damage regions (i.e. ANN configurations 1 to ***l***). Finally, the prediction error corresponding to ANNs with different configurations is compared to localise the damage.

A normalised mean error is defined to compare the prediction error in each region. This is essential since the recorded strains at target sensors and their associated errors may be in different ranges. Accordingly, the prediction error associated with the configured ANNs may not be directly comparable. In this paper, the normalised error is computed as:

$$NME(k,j) = \frac{\sum_{i=1}^{m} \frac{\varepsilon_{ANN}(i,j,k) - \varepsilon_{\exp}(i,k)}{\varepsilon_{\exp}(i,k)}}{m} \tag{6}$$

where $NME(k,j)$ is the normalised mean error associated with prediction of the $j^{th}$ ANN in configuration $k$, $\varepsilon_{exp}$ $(i,k)$ is FBG strain record at the target sensor of ANN

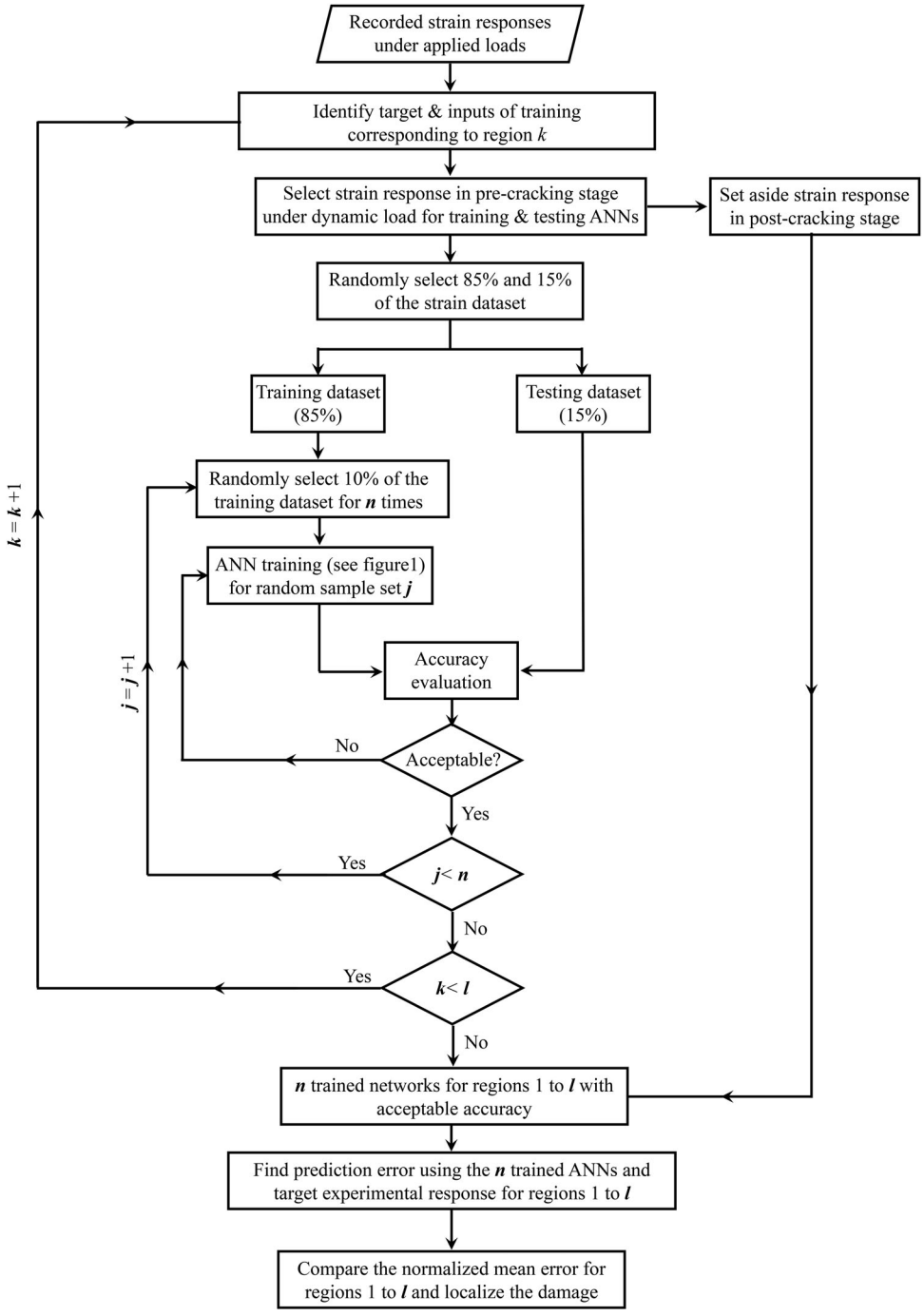


**Figure 3.** Layout of the proposed damage localisation approach.

configuration $k$ associated with the $i^{th}$ time instant, and $\varepsilon_{ANN}$ $(i,j,k)$ is the strain record at the target sensor of ANN configuration $k$ predicted by the $j^{th}$ ANN at time instant $i$.

## Illustrative example

The proposed damage detection procedure is illustrated on an approximately ½ scale AASHTO Type II prestressed girder. The beam was instrumented during construction with FBG sensors, vibrating wire strain gages (VWSGs), and a mid-span displacement sensor.

### Specimen design

The cross section of the tested girder consisted of two 13.2 mm diameter (0.52 in.) low-relaxation prestressing strands with minimum ultimate strength of 1860 MPa (270 ksi). The strands were tensioned to 75% of their specified tensile strength and placed 5 cm (2 in.) above the bottom fiber of the cross section. In addition, two No. 16 (#5) reinforcing bars were placed 5 cm (2 in.) below the top fiber of the cross section to counteract the concrete tensile stresses at time of prestress release. No. 10 (#3) Z-shaped bars were also placed transversely to resist shear stresses. Transverse shear reinforcement was designed to ensure flexural

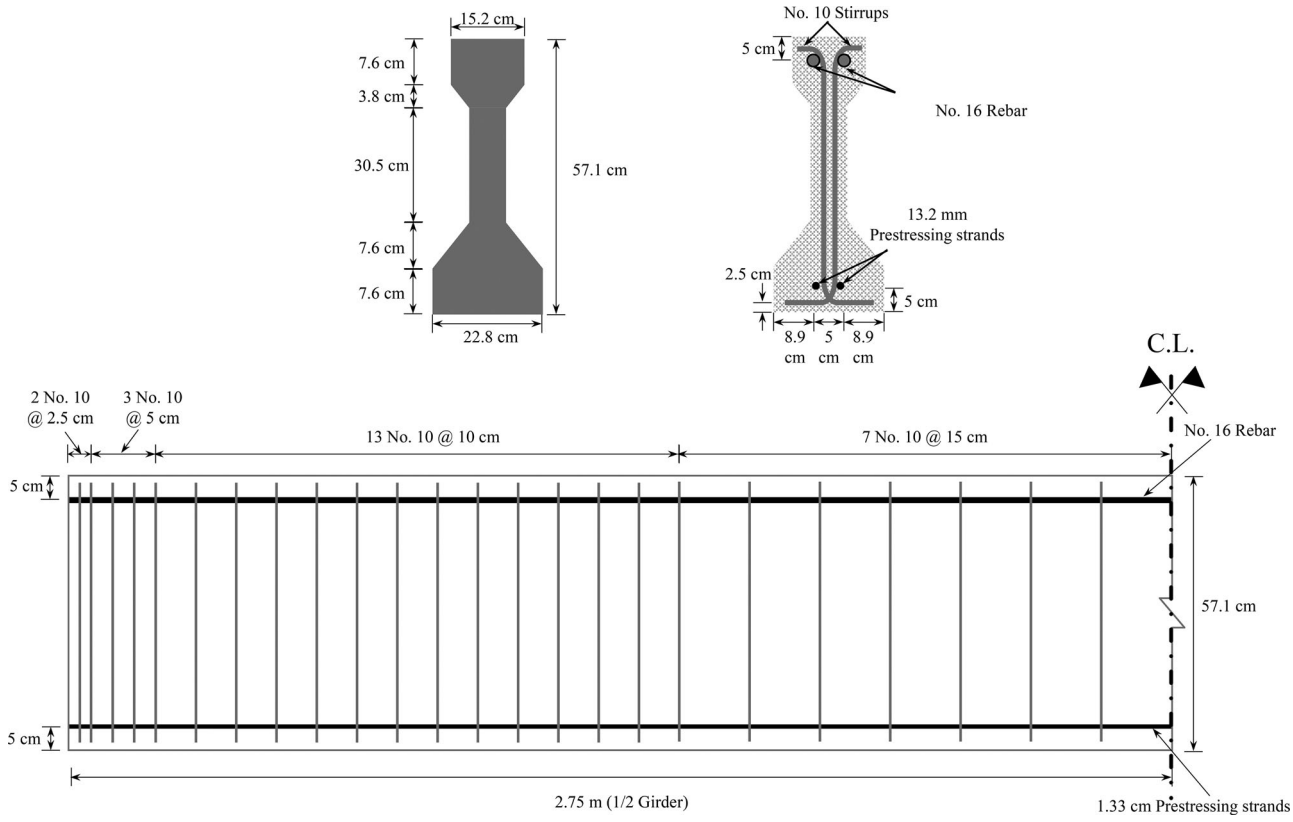


**Figure 4.** Geometry of the section and reinforcement details.

failure under a four-point-bending test. The beam was longitudinally symmetrical with respect to its mid-span. Figure 4 shows the geometry of the section, placement of reinforcement and prestressing strands, and spacing of shear reinforcement along one half of the beam. The girder was constructed using self-consolidating concrete designed to achieve a compressive strength of 27.5 MPa (4000 psi) and 55 MPa (8000 psi) at 7 and 28 days, respectively. Figure 5(a) and (b) shows, respectively, an elevation of the beam reinforcement and concrete placement process during the girder construction in Donald G. Fears Structural Engineering Laboratory located at the University of Oklahoma.

### *Temperature, deflection and strain monitoring using FBG sensors*

Two fiber optic cables, each consisting of 15 FBGs, were placed along the girder at the prestressing strand level. Each cable was placed to position 15 sensors in one half of the girder. A third fiber optic cable containing two temperature sensors, each in one half of the beam, was also embedded in the girder. The instrumentation was symmetric with respect to the centerline of the girder. Figure 6 shows the layout of the strain and temperature sensors (FBGs) distributed along one half of the beam. Note that the girder was longitudinally symmetrical. Clustering the sensors near the supports aimed at capturing the behaviour of the end regions during and after prestress transfer.

An interrogator featuring four channels and optimised for measuring static and dynamic measurements (FAZ Technology, 2019) was used to provide a source signal (i.e. laser light) for the fiber optic sensors and interpret the wavelength data under applied loads. The recorded change in wavelength from the strain and temperature sensors at different time instants during testing was then used to calculate the change in temperature and strain. Equation (7) presents the relationship between the temperature sensor reading and actual temperature in °C (FAZ Technology, 2019):

$$T_t = T_{S1}\left(\frac{\lambda T_t - \lambda T_{ref}}{\lambda T_{ref}}\right)^2 + T_{S2}\left(\frac{\lambda T_t - \lambda T_{ref}}{\lambda T_{ref}}\right) + T_{S3} \qquad (7)$$

where $T_t$ is the temperature in °C at time $t$, $T_{S1}$, $T_{S2}$, and $T_{S3}$ are temperature calibration coefficients provided by the manufacturer, while $\lambda T_t$ is the wavelength recorded by temperature sensor at time $t$ during the experiment, and $\lambda T_{ref}$ is the reference wavelength for the temperature sensor provided by the manufacturer.

The change in strain can be computed as (FAZ Technology, 2019):

$$\Delta\varepsilon_t = \frac{\frac{\lambda_t - \lambda_{initial}}{\lambda_{initial}} - B(T_t - T_{initial})}{A} \qquad (8)$$

in which $\Delta\varepsilon_t$ is change in strain at time $t$ with respect to initial strain value, $\lambda_{initial}$ and $T_{initial}$ are initial wavelength and temperature readings at the starting time of the test, and $\lambda_t$ and $T_t$ are wavelength and temperature reading at time $t$ during testing. $A$ and $B$ are calibration constants provided by the manufacturer. The values of the calibration parameters provided by the manufacturer are presented in Table 1.


**Figure 5.** View of (a) beam reinforcement before casting and (b) beam during construction.

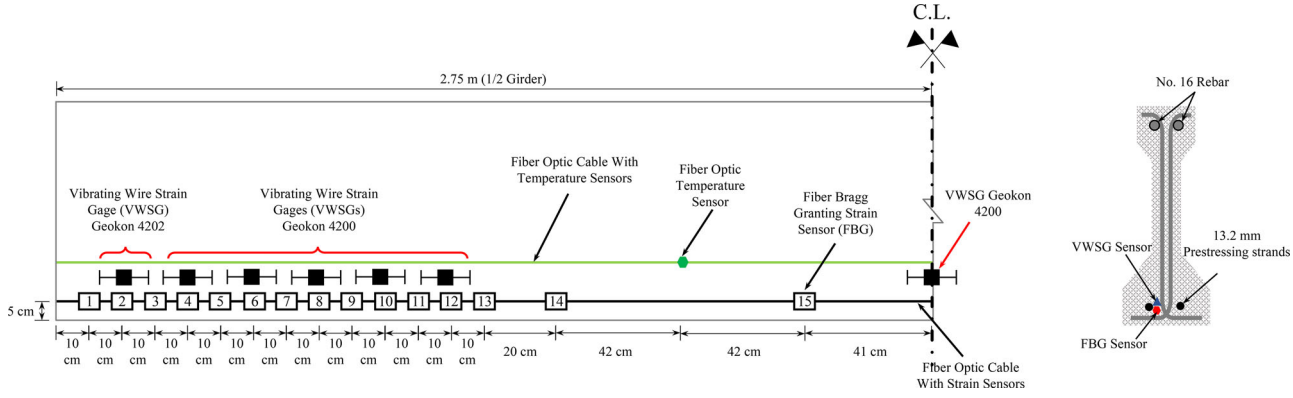


**Figure 6.** Layout of the FBGs and VWSGs distributed along one half of the beam.

**Table 1.** Calibration parameters for temperature and strain sensors.

| Calibration parameter | Temperature sensor 1 | Temperature sensor 2 | Strain sensors |
|---|---|---|---|
| $T_{S1}$ | −1,676,707.293078550 (°C) | 140,364.36897385 (°C) | — |
| $T_{S2}$ | 54,069.9715208757 (°C) | 53,482.2408014799 (°C) | — |
| $T_{S3}$ | 22.5024283936152 (°C) | 22.4751371210772 (°C) | — |
| $\lambda T_{ref}$ | 1557.486 (nm) | 1537.725 (nm) | — |
| A | — | — | 7.63625706E-07 ($\mu\varepsilon^{-1}$) |
| B | — | — | 5.96841206E-06 ($°C^{-1}$) |

### *Vibrating wire strain gages*

Thirteen VWSGs were also embedded in the girder during construction with six gages at each end and one at mid-span as shown in Figure 6. Two different models of VWSGs were used, Geokon 4200 and 4202 (Geokon, 2019) with 152 mm (6 in.) and 51 mm (2 in.) gage lengths, respectively. One Geokon 4202 strain gage with ±0.4 με measurement resolution and six Geokon 4200 gages with ±1 με resolution were distributed along each half of the specimen. The Geokon 4202 sensor was placed 10 cm (4 in.) away from the girder end while the Geokon 4200 sensors were distributed along the length of the beam as shown in Figure 6. In addition, a VWSG temperature sensor was attached externally to the girder surface to measure

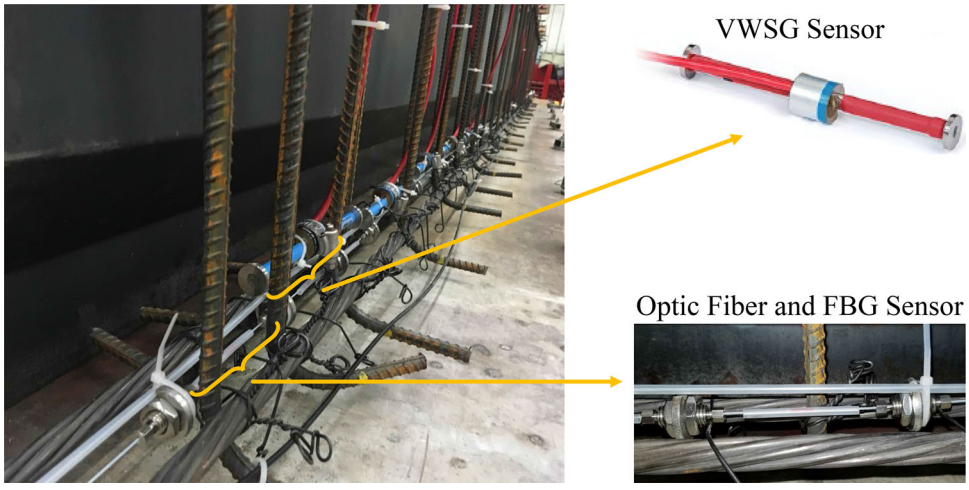


Figure 7. Placement of the FBGs and VWSGs in the constructed girder.

the ambient temperature during load tests. A single data-logger was used to record the VWSG sensor readings during testing. Figure 7 depicts the placement of FBG and VWSG sensors in the constructed girder.

### *Test procedure and loading*

The constructed girder was tested under four-point bending with load points 75 cm (30 in.) away from the mid-span. The point loads were applied through a spreader beam with two support points and a 250 kN (55 kip) hydraulic actuator with MTS FlexTest 60 load controller (MTS, 2019). Figure 8(a) and (b) shows the layout of the loading set up, and the actual test frame constructed in Bert Cooper Engineering Laboratory located at Oklahoma State University. The strain and temperature profiles during testing were recorded using the FBG sensors with 1000 Hz sampling frequency. The VWSG sensors were used to record strains during the monotonic tests. A sample from the VWSG sensors was recorded at each load increment. A linear variable displacement transducer (LVDT) was installed at mid-span to measure the beam deflections with 1000 Hz sampling frequency during all tests. The testing phase consisted of 19 loading runs, including 10 monotonic tests and 9 randomly generated dynamic load tests (i.e. variable amplitude loading). For the monotonic loading tests, the load was applied at a constant rate until a predefined maximum load level was reached; this maximum load was then kept constant for 5 minutes to allow beam inspection. Next, the specimen was unloaded at a constant rate of 13.4 kN/min (3 kip/min) until fully unloaded.

The experimental phase started with recording the response of the constructed prestressed girder under 3 different randomly generated variable amplitude dynamic loads and 4 monotonic loads (i.e. Dyna 1 to Dyna 3 and Mono 1 to Mono 4). Table 2 shows the attributes of different load runs. Note that the tests IDs are organised with respect to the order of conducting the tests. Next, another monotonic ramp load (i.e. Crack 1) was applied to the girder at 13.4 kN/min (3 kip/min) loading rate for the first 111 kN (25 kip) and with a reduced rate of 4.45 kN/m (1 kip/min) until the first crack was observed. During the Crack 1 load run, the loading was paused for two minutes at 4.45 kN (1 kip) increments to inspect the beam and identify the crack initiation. This process was continued until the first crack was observed at 160 kN (36 kip).

The cracking pattern in this stage can be seen in Figure 9. As shown, four cracks initiated and propagated to a level approximately 100 mm from the bottom fiber of the girder. This condition of the girder is referred to as the *minor cracking* state in this paper. Two more randomly generated dynamic loads runs (i.e. Dyna 4 and Dyna 5) were applied after the first minor cracking was observed. Next, another monotonic load (i.e. Crack 2) was applied to the girder. The load run was applied at 22.3 kN/min (5 kip/min) for the first 134 kN (30 kip) and continued at 4.45 kN/m (1kip/min) loading rate with a pause at each 4.45 kN (1 kip) until the cracks propagated to the upper half of the cross section at 191 kN (43 kip). The damage extent of the beam after this test is referred to as the *excessive cracking* state in this paper. The crack pattern in this stage is also shown in Figure 9. The experiment then continued with applying three more monotonic (i.e. Mono 5 to Mono 8) and four randomly generated dynamic loads (i.e. Dyna 6 to Dyna 9).

## Results and discussion

### *Concrete compressive strength*

Concrete compressive strength specimens for the girder were tested at 1, 7, and 28 days of age and before conducting the load tests at 69 days. Table 3 presents the average compressive strength of three cylinders tested at the aforementioned ages. The cracking and ultimate capacities of the beam were estimated based on the compressive strength test results, cross-sectional properties, and loading configuration to be 148 kN (33.4 kips) and 210 kN (47.2 kips), respectively. These capacities were used to design the loading procedure suitable for developing the proposed damage detection and localisation approach.

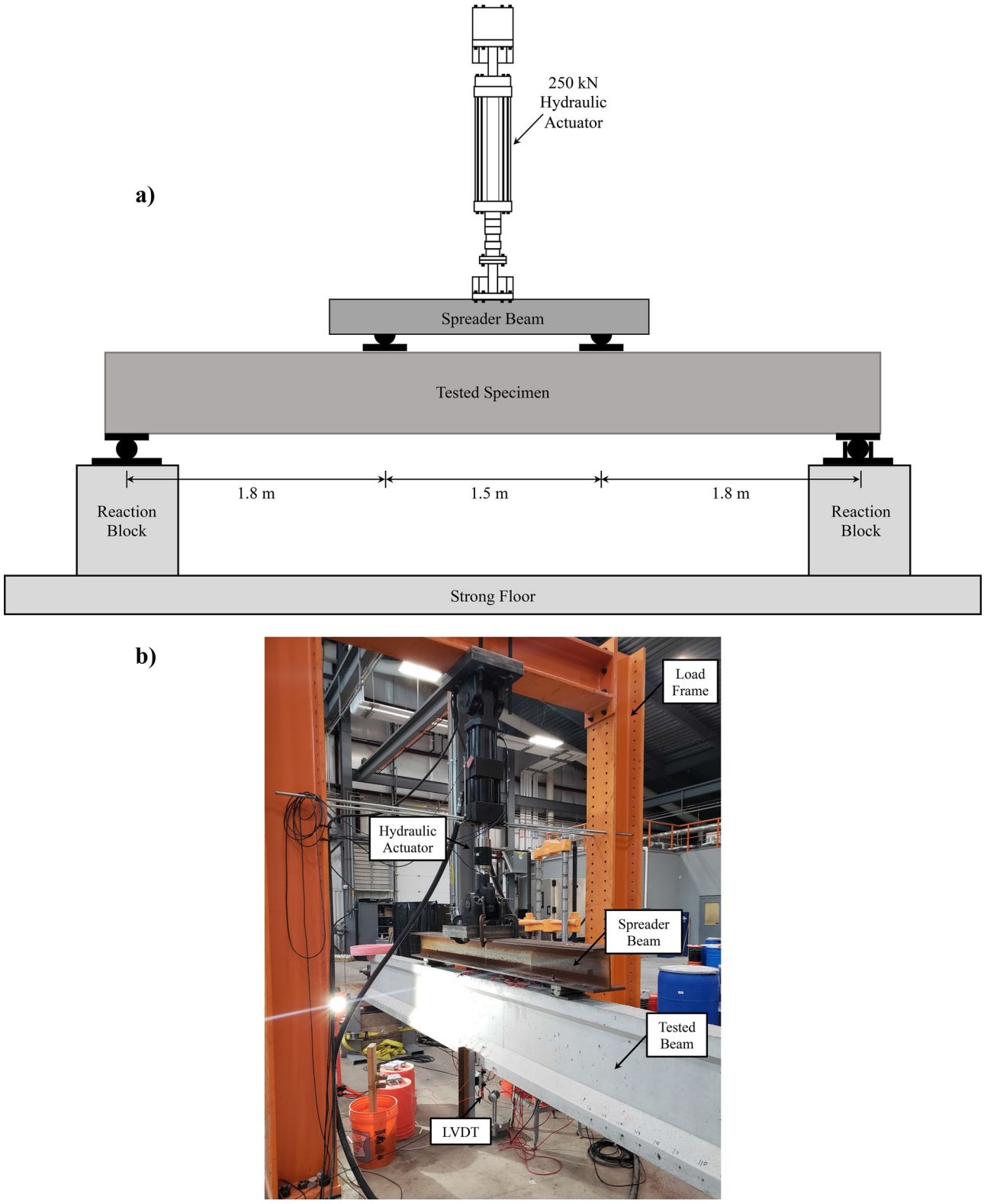


**Figure 8.** (a) Layout of the loading setup (b) test frame and the prestressed girder during load testing.

### *Load testing and strain measurement using FBGs and VWSGs*

As indicated previously, the FBG sensors distributed along the girder were used to obtain the strain time histories during monotonic and randomly generated dynamic load tests. Figure 10 displays the recorded response of sensor 15 during Dyna 3 load test. To ensure the proper operation of the fiber optic sensors, the strains recorded by the FBGs were compared to those obtained by the VWSGs during monotonic load tests. Figure 11 compares the change in strains obtained from FBG sensor 15 to those of the embedded VWSG at mid-span under various monotonic

Table 2. Attributes of different load tests.

| Test ID | Load type | Maximum load – kN (kip) | Frequency (Hz) | Loading rate – kN/min (kip/min) | Notes | Duration (seconds) |
|---|---|---|---|---|---|---|
| Dyna 1 | Random dynamic | 45 (10) | 2 | — | No cracks | 556 |
| Dyna 2 | Random dynamic | 62 (14) | 2 | — | No cracks | 695 |
| Dyna 3 | Random dynamic | 102 (23) | 2 | — | No cracks – training and testing dataset | 1200 |
| Mono 1 | Monotonic | 45 (10) | — | 13.4 (3) | No cracks | 440 |
| Mono 2 | Monotonic | 67 (15) | — | 13.4 (3) | No cracks | 640 |
| Mono 3 | Monotonic | 89 (20) | — | 13.4 (3) | No cracks | 840 |
| Mono 4 | Monotonic | 111 (25) | — | 13.4 (3) | No cracks | 1040 |
| Crack 1 | Monotonic | 160 (36) | — | Variable | First crack observed | 3000 |
| Dyna 4 | Random dynamic | 102 (23) | 2 | — | Small cracks | 1075 |
| Dyna 5 | Random dynamic | 107 (24) | 2 | — | Small cracks | 614 |
| Crack 2 | Monotonic | 191 (43) | — | Variable | Cracks widened | 2600 |
| Dyna 6 | Random dynamic | 107 (24) | 4 | — | Wide cracks | 321 |
| Dyna 7 | Random dynamic | 107 (24) | 6 | — | Wide cracks | 241 |
| Dyna 8 | Random dynamic | 107 (24) | 8 | — | Wide cracks | 175 |
| Dyna 9 | Random dynamic | 107 (24) | 10 | — | Wide cracks | 308 |
| Mono 5 | Monotonic | 89 (20) | — | 22.3 (5) | Wide cracks | 520 |
| Mono 6 | Monotonic | 134 (30) | — | 22.3 (5) | Wide cracks | 760 |
| Mono 7 | Monotonic | 156 (35) | — | 22.3 (5) | Wide cracks | 880 |
| Mono 8 | Monotonic | 180 (40) | — | 22.3 (5) | Wide cracks | 1000 |

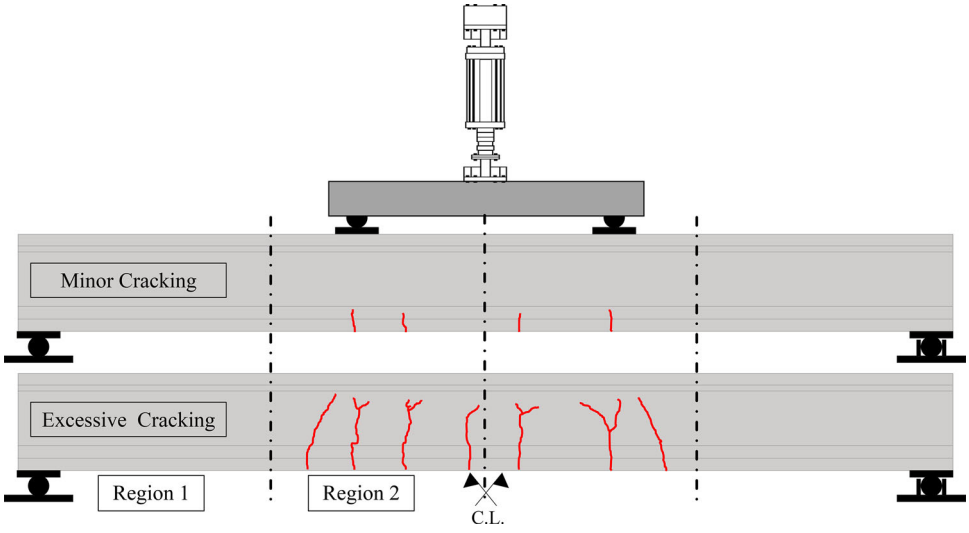


Figure 9. View of the beam showing minor and excessive cracking patterns.

Table 3. Concrete compressive strength test results.

| Concrete age (days) | Compressive strength – MPa (psi) |
|---|---|
| 1 | 31.7 (4600) |
| 7 | 47.4 (6870) |
| 28 | 52.9 (7670) |
| 69 (flexural testing) | 57.2 (8290) |

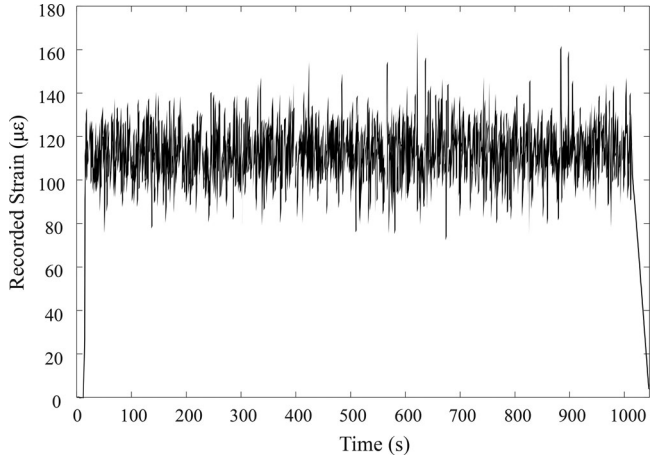


Figure 10. Recorded strain at sensor 15 during Dyna 3 load test.

load values. In summary, it was found that the FBG sensors provide a reliable and stable reading at different load levels.

## ANN training

Feed forward neural networks with 10 hidden neurons (see Figure 1) were used to establish the relationship between the strain readings of sensors along one half of the tested girder. Strain records associated with Dyna 3 load run were randomly divided into training and testing datasets representing 85% and 15% of the data points, respectively. These percentages which are initially selected based on the common practice of ANN applications (e.g. Ezeldin & Sharara, 2006; Khandel & Soliman, 2019) were evaluated to make sure both the datasets have similar statistical properties. Note that any other strain record under dynamic loads in the pre-cracking stage (e.g. Dyna 1 or Dyna 2) can be used for training the ANNs. The strain records of eight sensors, namely 1, 2, 3, 10, 11, 12, 13, and 14 along one half of the beam were used as the input to predict the strains at target sensor 15.

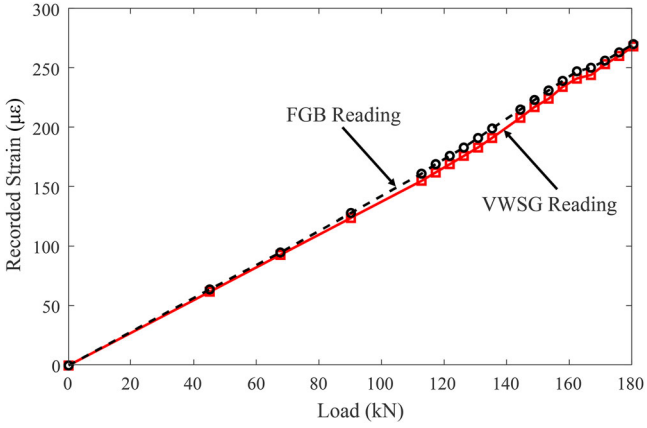


**Figure 11.** Comparison between the measured strains using FGB sensor 15 and the embedded VWSG at mid-span under various monotonic load values.

Given the large size of the training dataset, statistical analysis was performed, and it was found that a randomly selected 10% of the data can properly represent the statistical properties of the whole training database. However, higher percentage of the training dataset may be needed for other applications. Accordingly, for training each individual ANN, 10% of the training database was randomly selected and used for training. The accuracy of each ANN was then evaluated using the testing database. In order to account for modelling uncertainty associated with ANN predictions, 1000 individual ANNs were trained in this example.

Levenberg-Marquardt (Levenberg, 1944; Marquardt, 1963) optimisation method was employed to obtain the fitting parameters that minimise the mean square error (MSE) between the predicted strains and the defined target dataset by optimising the fit parameters in Equation (1). The ANNs were created and trained using the MATLAB (MathWorks, 2019) neural network toolbox. For damage detection and localisation, the strain readings of the input sensors from the other load tests were then fed to the 1000 trained ANNs and the strain time histories for the target sensor were predicted.

### Error estimation

The error between the experimentally- and ANN-generated strains was estimated for the testing dataset to evaluate the performance of the trained neural networks. The prediction error associated with individual ANNs was found using Equation (2) while the mean, lower bound, and upper bounds of the strain prediction error were estimated using Equations (3) (4), and (5), respectively. Figure 12(a) presents the probability distribution of the prediction error, as well as the mean ($ME$), lower bound ($E_{LB}$), and the upper bound error ($E_{UB}$). The mean prediction error was estimated to be very close to zero (7.2823e-04 με), the standard deviation was estimated as 0.1905 με, whereas the lower and upper bounds at 95% confidence intervals were −0.3825 and 0.3846 με, respectively.

The small mean error value shows that trained ANNs were able to simulate the behaviour of the girder in the pre-cracking state with high accuracy. In addition, there is 95% confidence that the error in the pre-cracking stage falls within the calculated lower and upper bounds. Figure 12(b) shows the ME prediction versus the number of ANNs used to monitor convergence of the proposed framework. As shown, the fluctuation of the mean prediction error is stabilised and limited to approximately 0.00015 με after employing 200 ANNs. A similar trend was also observed for convergence of the lower and upper prediction error. This can imply that the number of employed ANNs and the size of training dataset was adequate to accurately predict the flexural behaviour of the tested girder.

### Damage detection

After training the ANNs and evaluating the prediction error, the strain records of sensors 1, 2, 3, 10, 11, 12, 13, and 14 from the set-aside datasets were fed to the trained ANNs and the resulting strain at sensor 15 was predicted. The predicted strains were then compared to the ones recorded during the load tests and the associated mean error was calculated using Equation (3) to predict the damage occurrence.

Figure 13 compares the experimental strain time history to ANN predictions at sensor 15 for two load cases in the pre-cracking (i.e. Dyna 2 test) and post-cracking phases (i.e. Dyna 6 test). As shown, the trained ANNs were able to accurately predict the strains in the pre-cracking stage, while there seems to be a significant prediction error associated with the post-cracking stage. In other words, the predicted strains at the target sensor are considerably different than the recorded ones. This implies that it is highly likely that damage has occurred. This is based on the fact that due to damage in the post cracking stage, the stiffness of the system changes compared to the pre-cracking state and the relationship between different sensors, established in the uncracked state, leads to an increase in the ANN prediction error.

Figure 14(a) shows the mean prediction error for the randomly generated variable amplitude load tests. This figure is divided into three zones, *no cracking*, *minor cracking*, and *excessive cracking*. Referring to Table 2, Tests Dyna 1 and Dyna 2 were conducted before cracking the girder, while Tests Dyna 4 and Dyna 5 occurred after load test Crack 1 that resulted in the initiation of minor cracking. Finally, Test Dyna 6 to Dyna 9 were conducted after applying the Crack 2 loading, in which cracks increased in width and length. In the *no crack* zone, the two data points fall within the previously defined upper and lower bounds of prediction error ($E_{UB}$ and $E_{LB}$). In the other two regions, the prediction error falls outside of the defined criteria indicating the presence of damage in the beam. This highlights the ability of the proposed criterion to detect the damage occurrence. In addition, the large difference between the $ME$ values in the minor and excessive cracking regions shows that the proposed approach can indicate the relative level of damage experienced by the girder during load tests.

Figure 14(b) provides a comparison between the mean prediction error associated with different monotonic load tests. The insert in the no cracking zone highlights the

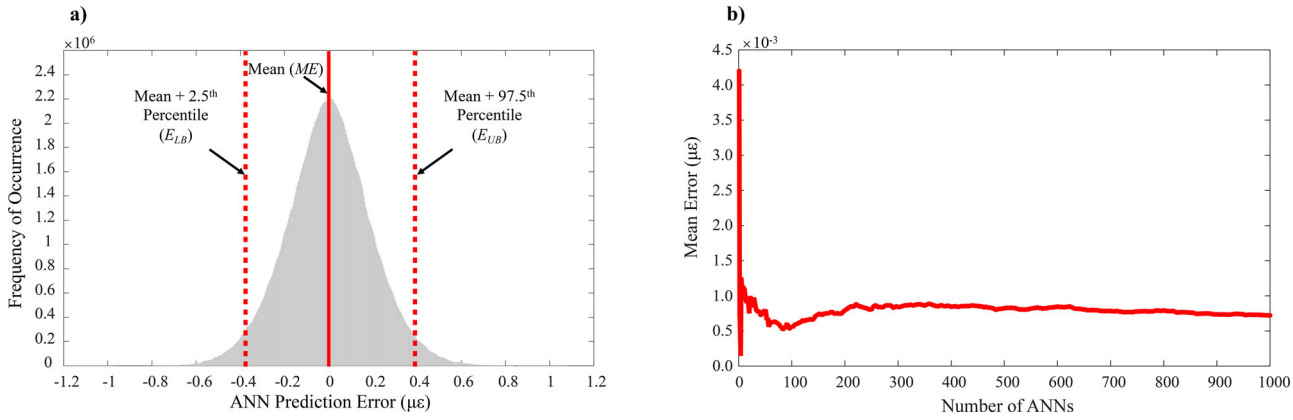


**Figure 12.** (a) Probability distribution of the prediction error (*E*), mean error (*ME*), lower bound error ($E_{LB}$), and upper bound error ($E_{UB}$) associated with the testing dataset (b) mean error convergence plot.

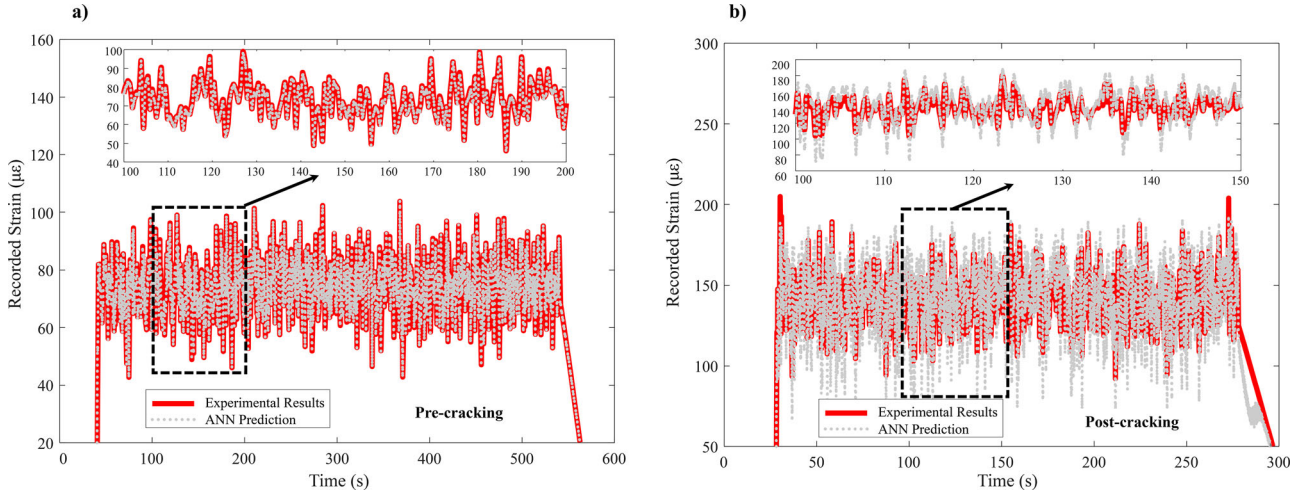


**Figure 13.** Comparison between experimental results and ANN predictions for two load cases in (a) pre-cracking and (b) post-cracking phases.

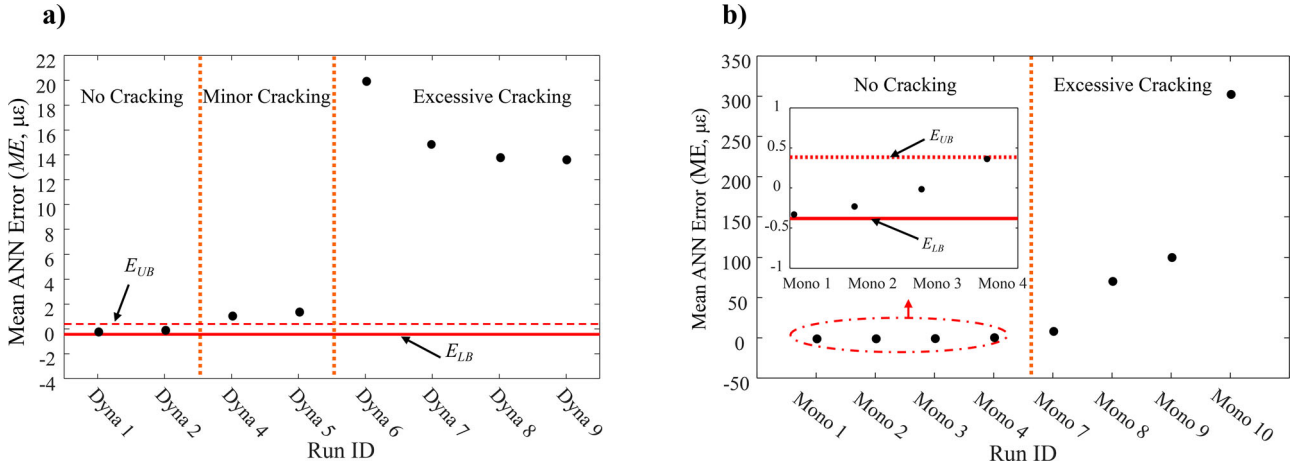


**Figure 14.** Mean prediction error for (a) randomly generated variable amplitude load cases (b) monotonic load tests.

mean prediction error in the first four monotonic runs with respect to the upper and lower bounds. The *ME* values associated with monotonic load tests applied before crack initiation (i.e. Mono 1 to 4) fall within the defined bounds, where the *ME* values for the other cases fall outside of the defined bounds indicating the presence of damage. As shown, larger monotonic loads resulted in larger mean error values. This can be mainly attributed to the fact that larger loads caused larger crack opening and resulted in larger error compared to the ANN prediction. Note that the specimen was designed to be a fully prestressed with no cracking under service loads. The presented approach can be adapted to partially prestressed beams by relaxing the bounds on prediction errors to permit allowable cracking and isolate excessive cracking. However, more testing may be needed on such cases to establish these new bounds.

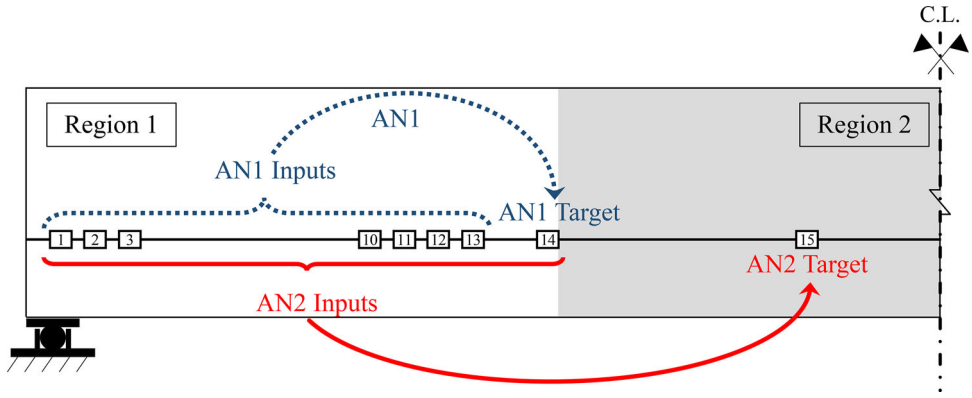


**Figure 15.** Visualisation of AN1, AN2, Region 1, and Region 2.

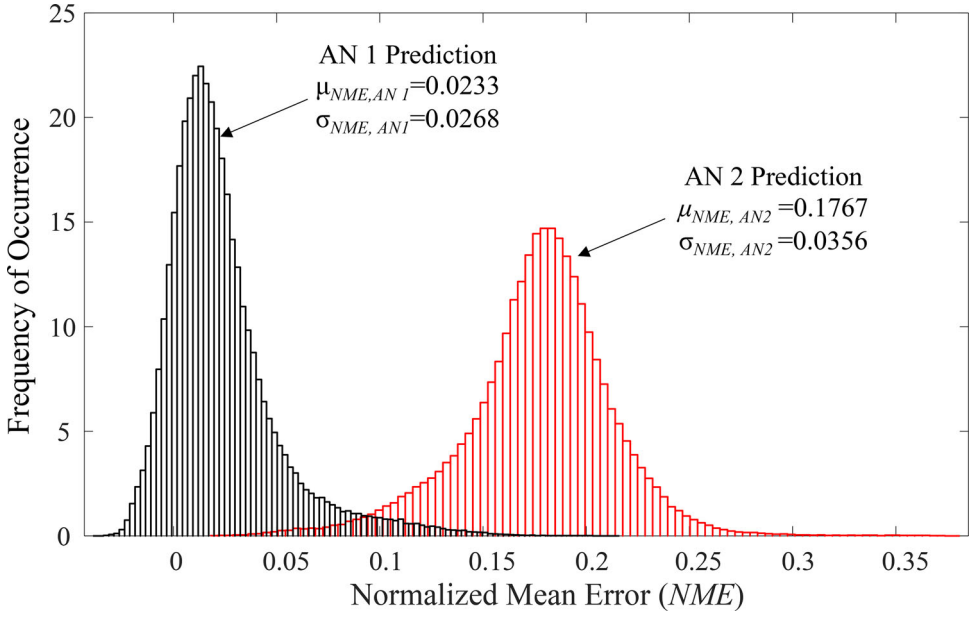


**Figure 16.** Probability distribution of the calculated *NME* values associated with AN1 and AN2.

### *Damage localisation*

In order to localise damage in the tested girder, two damage regions and ANN configurations were defined and trained using the strain records of Dyna 3 load test. Region one was considered to span between the support and sensor 14 (1.5 m [59 in.] away from the beam end), and region two was defined to be between sensors 14 and mid-span (i.e. 1.25 m [49 in.] away from the mid-span). ANN with configuration 1 (AN 1) used the strain records of sensors 1, 2, 3, 10, 11, 12, and 13 to predict the strain in sensor 14, and ANN with configuration 2 (AN 2) was the same configuration introduced in the damage detection process.

Figure 15 illustrates the defined regions and their associated sensors. These configurations are suitable for predicting flexural damage in the tested beam; however, other configurations may be needed to localise damage if other failure modes are expected. The prediction error of each ANN based on Dyna 6 load test was then used to localise damage along the beam. The normalised mean error (NME) associated with the prediction of AN1 and AN2 configurations was found using Equation (6) and Dyna 6 load test data. Figure 16 shows the probability distribution of the calculated NME values associated with 1000 AN1 and AN2 trained ANNs. The mean and standard deviation of the predicted NME for AN1 are 0.0233 and 0.0268, respectively. While the mean and standard deviation for AN2 are found to be 0.1767, and 0.0356, respectively. This shows that the established relationship between the sensor readings in Region 1 (see Figure 15) can predict the strains in the post-cracking phase with ±2.3% mean error.

However, the 17.67% NME for AN2 reveals that the established relationship between the sensors in Region 2 (see Figure 15) cannot accurately simulate the strains in the post-cracking phase. Accordingly, it is more likely that the cracks occurred in Region 2. This conclusion is also consistent with the observations made during the experiment, where the cracks initiated and propagated in the pure bending zone (see Figure 9).

## Conclusions

This paper presented a statistical damage detection and localisation approach for evaluating the long-term performance of newly constructed prestressed concrete girders instrumented with fibre Bragg grating sensors. The approach was illustrated using experimental laboratory data obtained

from flexural testing of a large-scale prestressed concrete girder under monotonic loads and randomly generated variable amplitude loading. ANNs were employed to establish a relationship between the strain time-histories at multiple sensors distributed along the girder. The trained ANNs were used to predict strain at a target sensors based on the readings of other sensors during a load test.

The predicted strains were then compared to their experimental counterparts for damage assessment. Lower and upper error bounds were defined based on the intact girder conditions. These bounds were then used to evaluate the condition of the investigated prestressed concrete girder and localise induced damage. The proposed damage detection approach does not require any information on loading conditions and detects the damage based only on the relationship between different FBG signals. The following conclusions are drawn:

- The employed feedforward ANNs with the adopted characteristics were capable of establishing a relationship between strain readings recorded at various sensors along the tested girders. The predication accuracy was highlighted by low mean error and standard deviation of 7.2823e-04 με and 0.1905 με, respectively.
- The proposed lower and upper error bounds led to successful detection of various damage levels. The approach was able to identify the occurrence of minor and excessive cracking during testing. The identified damage levels were consistent with observations made during testing. The load tests conducted on the heavily cracked beam showed a large mean error while tests at early cracking stages showed relatively small mean error values that were still out of the defined bounds.
- The proposed damage localisation approach was capable of identifying the region that experienced higher damage levels. The identified damage zone matched the observations made during the experimental testing. However, more research is needed to optimise sensor placement and region selection.
- The presented approach has been validated for flexural damage in fully prestressed simply supported beams. More research is needed to quantify the effect of loading location, temperature gradients, boundary conditions, and shrinkage and creep strains on the proposed approach. Additionally, future efforts are required to implement the presented damage identification and localisation approach for long-term performance monitoring of bridges under field conditions.

## Acknowledgements

The opinions and conclusions presented in this paper are those of the authors and do not necessarily reflect the views of the sponsoring organisations.

## Disclosure statement

No potential conflict of interest was reported by the authors.

## Funding

The authors gratefully acknowledge the financial support from (a) the Southern Plains Transportation Center (SPTC) project number 17.1-01A and (b) the National Science Foundation (NSF) Award OAC-1835371.

## ORCID

Omid Khandel https://orcid.org/0000-0003-2204-340X
Mohamed Soliman https://orcid.org/0000-0003-3160-0933
Cameron D. Murray http://orcid.org/0000-0002-7392-7849

## References

Abdel-Jaber, H., & Glisic, B. (2015). Analysis of the status of pre-release cracks in prestressed concrete structures using long-gauge sensors. *Smart Materials and Structures*, *24*(2), 025038. doi:10.1088/0964-1726/24/2/025038

Abdel-Jaber, H., & Glisic, B. (2019). Monitoring of long-term prestress losses in prestressed concrete structures using fiber optic sensors. *Structural Health Monitoring*, *18*(1), 254–269. doi:10.1177/1475921717751870

Anastasopoulos, D., De Smedt, M., Vandewalle, L., De Roeck, G., & Reynders, E. P. (2018). Damage identification using modal strains identified from operational fiber-optic Bragg grating data. *Structural Health Monitoring*, *17*(6), 1441–1459.

Butler, L. J., Gibbons, N., He, P., Middleton, C., & Elshafie, M. Z. (2016). Evaluating the early-age behaviour of full-scale prestressed concrete beams using distributed and discrete fibre optic sensors. *Construction and Building Materials*, *126*, 894–912. doi:10.1016/j.conbuildmat.2016.09.086

Chung, W., & Kang, D. (2008). Full-scale test of a concrete box girder using FBG sensing system. *Engineering Structures*, *30*(3), 643–652. doi:10.1016/j.engstruct.2007.05.003

Dunphy, J. R., Meltz, G., Lamm, F. P., & Morey, W. W. (1990). Multifunction, distributed optical fiber sensor for composite cure and response monitoring. In *Fiber optic smart structures and skins III* (Vol. 1370, pp. 116–118). Bellingham, WA: International Society for Optics and Photonics. doi:10.1117/12.24834

Ezeldin, A. S., & Sharara, L. M. (2006). Neural networks for estimating the productivity of concreting activities. *Journal of Construction Engineering and Management*, *132*(6), 650–656. doi:10.1061/(ASCE)0733-9364(2006)132:6(650)

FAZ Technology. (2019). Retrieved from http://www.faztechnology.com

Federal Highway Administration (FHWA). (2016). National bridge inventory (NBI) dataset. Retrieved from https://www.fhwa.dot.gov/bridge/nbi/ascii2016.cfm

Geokon. (2019). Retrieved from https://www.geokon.com/

Gres, S., Ulriksen, M. D., Döhler, M., Johansen, R. J., Andersen, P., Damkilde, L., & Nielsen, S. A. (2017). Statistical methods for damage detection applied to civil structures. *Procedia Engineering*, *199*, 1919–1924. doi:10.1016/j.proeng.2017.09.280

Hagan, M. T., & Menhaj, M. B. (1994). Training feedforward networks with the Marquardt algorithm. *IEEE Transactions on Neural Networks*, *5*(6), 989–993. doi:10.1109/72.329697

Idriss, R. L., Kodindouma, M. B., Kersey, A. D., & Davis, M. A. (1998). Multiplexed Bragg grating optical fiber sensors for damage evaluation in highway bridges. *Smart Materials and Structures*, *7*(2), 209–216. doi:10.1088/0964-1726/7/2/008

Inaudi, D., & Vurpillot, S. (1999). Monitoring of concrete bridges with long-gage fiber optic sensors. *Journal of Intelligent Material Systems and Structures*, *10*(4), 280–292. doi:10.1177/1045389X9901000404

Jin, S. S., & Jung, H. J. (2018). Vibration-based damage detection using online learning algorithm for output-only structural health

monitoring. *Structural Health Monitoring*, *17*(4), 727–746. doi:10.1177/1475921717717310

Kang, L. H., Kim, D. K., & Han, J. H. (2007). Estimation of dynamic structural displacements using fiber Bragg grating strain sensors. *Journal of Sound and Vibration*, *305*(3), 534–542. doi:10.1016/j.jsv.2007.04.037

Khandel, O., & Soliman, M. (2019). *Deep learning based framework for long-term management of bridges considering climate change effects*. Proceeding of 2019 IABSE Congress, New York City, NY.

Levenberg, K. (1944). A method for the solution of certain non-linear problems in least squares. *Quarterly of Applied Mathematics*, *2*(2), 164–168. doi:10.1090/qam/10666

Lin, Y. B., Chang, K. C., Chern, J. C., & Wang, L. A. (2004). The health monitoring of a prestressed concrete beam by using fiber Bragg grating sensors. *Smart Materials and Structures*, *13*(4), 712–718. doi:10.1088/0964-1726/13/4/008

Marquardt, D. W. (1963). An algorithm for least-squares estimation of nonlinear parameters. *Journal of the Society for Industrial and Applied Mathematics*, *11*(2), 431–441. doi:10.1137/0111030

MathWorks. (2019). MATLAB: The language of technical computing. Retrieved from https://www.mathworks.com/help/matlab

Mattson, S. G., & Pandit, S. M. (2006). Statistical moments of autoregressive model residuals for damage localisation. *Mechanical Systems and Signal Processing*, *20*(3), 627–645. doi:10.1016/j.ymssp.2004.08.005

Mehta, A. (2019). A complete guide to types of Neural Networks. Retrieved from https://www.digitalvidya.com/blog/types-of-neural-networks/

Montana, D. J., & Davis, L. (1989). Training feedforward neural networks using genetic algorithms. *IJCAI*, *89*, 762–767.

Morey, W. W., Meltz, G., & Glenn, W. H. (1990). Fiber optic Bragg grating sensor. In *Fiber optic and laser sensors VII* (Vol. 1169, pp. 98–107). Bellingham, WA: International Society for Optics and Photonics. doi:10.1117/12.963022

MTS. (2019). Retrieved from https://www.mts.com

Prohaska, J. D., Snitzer, E., Chen, B., Maher, M. H., Nawy, E. G., & Morey, W. W. (1993). Fiber optic Bragg grating strain sensor in large-scale concrete structures. In *Fiber optic smart structures and skins V* (Vol. 1798, pp. 286–294). Bellingham, WA: International Society for Optics and Photonics.

Reiff, A. J., Sanayei, M., & Vogel, R. M. (2016). Statistical bridge damage detection using girder distribution factors. *Engineering Structures*, *109*, 139–151. doi:10.1016/j.engstruct.2015.11.006

Santos, J. P., Crémona, C., Orcesi, A. D., & Silveira, P. (2013). Multivariate statistical analysis for early damage detection. *Engineering Structures*, *56*, 273–285. doi:10.1016/j.engstruct.2013.05.022

Uva, G., Porco, F., Fiore, A., & Porco, G. (2014). Structural monitoring using fiber optic sensors of a pre-stressed concrete viaduct during construction phases. *Case Studies in Nondestructive Testing and Evaluation*, *2*, 27–37. doi:10.1016/j.csndt.2014.06.002

Waeytens, J., Rosić, B., Charbonnel, P.-E., Merliot, E., Siegert, D., Chapeleau, X., … Cottineau, L.-M. (2016). Model updating techniques for damage detection in concrete beam using optical fiber strain measurement device. *Engineering Structures*, *129*, 2–10. doi:10.1016/j.engstruct.2016.08.004

Webb, G. T., Vardanega, P. J., Hoult, N. A., Fidler, P. R. A., Bennett, P. J., & Middleton, C. R. (2017). Analysis of fiber-optic strain-monitoring data from a prestressed concrete bridge. *Journal of Bridge Engineering*, *22*(5), 05017002. doi:10.1061/(ASCE)BE.1943-5592.0000996

Weinstein, J. C., Sanayei, M., & Brenner, B. R. (2018). Bridge damage identification using Artificial Neural Networks. *Journal of Bridge Engineering*, *23*(11), 04018084. doi:10.1061/(ASCE)BE.1943-5592.0001302

Zhang, W., Gao, J., Shi, B., Cui, H., & Zhu, H. (2006). Health monitoring of rehabilitated concrete bridges using distributed optical fiber sensing. *Computer-Aided Civil and Infrastructure Engineering*, *21*(6), 411–424. doi:10.1111/j.1467-8667.2006.00446.x